

FINITE ELEMENT MODELLING AND SIMULATION OF CHIP BREAKING WITH GROOVED TOOL

Deng, W. J.; Xie, Z. C.; Li, Q. & Lin, P.

School of Mechanical and Automotive Engineering, South China University of Technology,
Guangzhou 510641, China

E-Mail: dengwj@scut.edu.cn

Abstract

A finite element model is presented to simulate chip breaking when orthogonal turning medium carbon steel with a grooved cutting tool is used. The chip formation, chip breaking, cutting force, stress, strain and temperature are simulated by the thermo-elastic-plastic finite element method, using commercial finite element software. The cutting process is simulated from the initial to the steady-state of cutting force, and then to periodic fractures of machined chip, by incrementally advancing the cutting tool. Normalized Cockcroft & Latham's criterion is employed to predict the effect of tensile stress on chip fracture. The cutting force and bending moment are analysed to explain the mechanism of chip breaking. Experiments on the application of the grooved cutting tool were performed. The simulated broken chip profile and cutting force compare well with experimental observations that the established FE model is capable of capturing the overall trend of the experimental results.

(Received in January 2013, accepted in May 2013. This paper was with the authors 2 months for 1 revision.)

Key Words: Orthogonal Machining, Chip breaking, Grooved Tool, FEM, Chip Fracture Criterion

1. INTRODUCTION

Machining is a most frequently employed manufacturing operation to remove unnecessary materials from workpiece and to form desirable shapes with dimensional accuracy. Proper chip control during the machining of metals is a major concern in automated machining operations [1]. The long, continuous chips generated in machining can lead to problems of scratching on the surface of the finished workpiece, loss of production time, rapid tool wear and failure. The basic functions of chip control are efficient breaking and effective removal of chips. Breaking chips into suitable length during continuous machining is an important aspect in machining. There is, therefore, a need for a comprehensive and systematic understanding of chip control, including chip flow, curl and breaking. Balaji et al. [2] presented recent developments in chip control and provided major applications in turning operations. Lee et al. [3] developed a new chip-breaking index, defined based on the thickness and length of the broken chip, to assess chip-breaking characteristics in turning operations. Grzesik and Kwiatkowska [4] presented a better understanding of chip-breaking and performed experiments to measure the cutting force, cutting energy and the temperature at the chip-tool interface together with identification of the chip form.

During the chip breaking process, the chip flow direction and the tool configuration heavily influence the chip curl and subsequent chip breaking. Chip breakers are utilized to control the chip flow and curl. In obstruction chip breakers, the naturally curled chip after reaching the tool-chip natural contact length is further curled by the action of the tool face obstruction. However, for the grooved chip formers, the chip flows into the groove due to the

effect of tool restricted contact and then is curled by the groove back-wall. Utilizing an obstruction or groove type chip breaker is an effective approach to promote chip breaking. Radius of the chip curvature can be controlled and bending strain inside the chip induces a break. Kim and Kweun [5] provided useful information on the chip-breaker design and on the experimental cutting of mild steel with the chip breaker. The characteristics of chip breakage for mild steel with respect to cutting speed, depth of cut and feed were analysed from the experimental results. Alvarez et al. [6] analysed the effect of eight constitutive models on the saw-toothed chip formation in Ti6Al4V orthogonal cutting, by means of the finite element (FE) simulation and experimental comparison. A critical comparison of outstanding process outputs such as cutting force, temperature on rake face and measurable parameters for segmented chip (the peak tooth height, the valley tooth height and the tooth width, chip compression ratio, and chip deformation) was carried out. Fang [7] investigated systematically and comprehensively the influence of the geometrical parameters of the chip groove on the chip-breaking performance. The geometrical parameter of the chip groove influenced the minimum feed and cut of depth for chip breaking. Besides, Zhou et al. [8] established a semi-empirical model of machining chip breaking limits.

The types of chips produced in machining depend on the geometry of the cutting tool, cutting conditions and the workpiece materials. Puh et al. [9] used Taguchi method to find optimum process parameters for hard turning of hardened steel AISI 4142 using PCBN tool. Athavale and Strenkowski [10] presented a chip breaking model for orthogonal cutting and found that both chip geometry and chip ductility influences chip breakability. Kamiya and Yakou [11] performed turning tests for various wrought aluminium alloys to evaluate chip breakability. Aluminium alloys containing second-phase particles showed good chip breakability. Joshi et al. [12] attempted to understand the machining characteristics of Al/SiCp composite material. The chip breaking phenomenon was related to the mechanical properties of composites.

Finite element modelling and simulation is an effective approach in understanding chip formation because of possibility of numerically modelling different types of metal machining problems. Entire complicated processes can be automatically simulated, thus avoiding the need for repetitive trial and error experiments for tool design and chip breaking investigation. Gyliene and Ostasevicius [13] presented experimental and numerical study of the end-milling process, aiming at defining the force acting on a single cutting tool insert. A finite element model of the milling process was designed to determine the residual stress distribution across the depth of the machined surface. Tamizharasan and Senthil Kumar [14] attempted to minimize flank wear of uncoated carbide inserts by finite element modelling and simulation. The effect of tool geometries on performance measures of flank wear, surface roughness and cutting forces generated were evaluated. Chaari et al. [15] presented a contribution for modelling and quantification of the machining geometric defects, considering machining dynamic effects. A method was developed based on Homogeneous Transformation Method. The dynamic displacements due to clamping and machining forces were defined using Finite Element Method. Ganapathy and Jawahir [16] proposed a new cutting force model incorporating the contact force developed due to the free-end of the chip touching the workpiece. The model was applicable to study the 2D chip breaking in orthogonal machining. Results showed that the forces acting on the chip vary within a chip breaking cycle and help identify the chip breaking event. Fang and Jawahir [17] provided a full analytical model to predict the cyclic chip formation and the relevant process variables in 2-D machining with chip breaking. This model included a chip/work contact force at the free-end of the curled chip which contributes to the development of a bending moment in the chip. Shinozuka et al. [18] simulated the process of the chip breaking and the change of the forces acting at the chip

breaker edge of the arbitrary rake face geometry tool under various cutting conditions using finite element modelling and simulation.

In this paper, the commercial finite element software Defrom-2D is adopted to simulate chip breaking during machining using a grooved cutting tool. The cutting force, stress, strain and temperature during chip breaking are obtained. Normalized Cockcroft & Latham's criterion is employed to predict the effect of tensile stress on chip fracture. The cutting force and bending moment are analysed to study the mechanism of chip breaking.

2. FINITE ELEMENT MODELLING

2.1 Meshing model and boundary conditions

The finite element model used for orthogonal machining simulation was based on the Lagrangian implicit code of the commercial FEA software DEFORM-2D. The plane-strain assumption was used as a reasonable approximation. In real metal machining the width of cut was at least five times greater than the depth of cut; therefore, the chip was produced under nearly plane-strain conditions.

Fig.1 (a) shows the dimensions and the initial finite element mesh of the workpiece and the tool. The workpiece was initially meshed with 6382 elements. A very fine mesh density was defined at the upper part of the workpiece to obtain accurate prediction of the chip formation and breaking. The tool, modelled as being rigid and subjected only to heat transfer analysis, was divided into 829 elements. A very fine mesh density was defined at the tip of the tool and at the contact zone to obtain fine temperature distributions. Automatic adaptive remeshing procedure was performed frequently to deal with large deformation.

As shown in Fig.1 (b), the bottom edge (BC) of the workpiece was constrained in all directions. The tool was fixed in the vertical direction and was allowed to move horizontally. The machining process was eventually produced by applying a horizontal displacement boundary condition on the tool. The tool moved into the workpiece at a given cutting speed. The cutting speed could be changed by assigning different displacement boundary conditions.

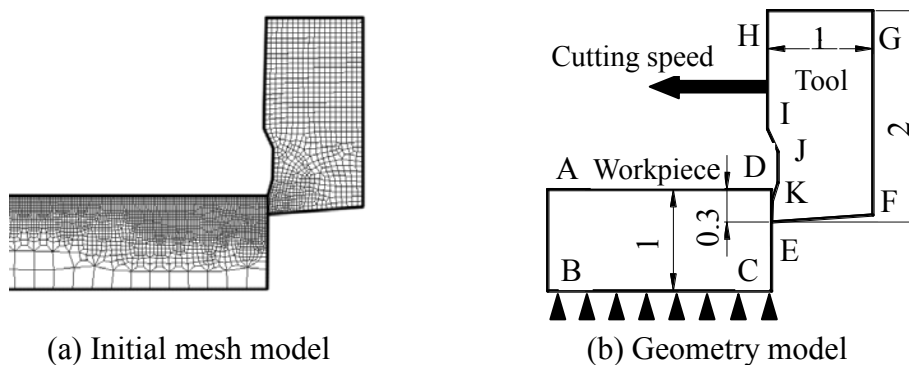


Figure 1: Mesh and geometry models of chip breaking simulation.

A tool with grooved chip breaker was chosen. The geometrical parameters of the grooved chip breaker consisted of the rake land length L , the groove width W , the groove depth H , the groove back-wall height h , the rake angle γ_0 and the clearance angle α_0 , as shown in Fig. 2. The tool dimensions were as follows: $L = 0.2$ mm, $W = 0.7$ mm, $H = 0.1$ mm and $h = 0.05$ mm. The cutting conditions used for the orthogonal machining simulation were: $\gamma_0 = 15^\circ$, $\alpha_0 = 5^\circ$, cutting speed $v = 60$ m/min and feed $f = 0.3$ mm/rev.

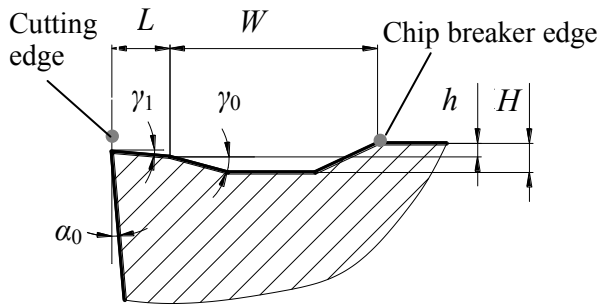


Figure 2: Geometrical parameters of the chip groove.

2.2 Workpiece and tool material modelling

The workpiece material used for the orthogonal machining simulation was medium steel AISI1045 with 0.43-0.50 % C, Poisson's ration 0.3. The temperature dependent physical properties of the material are shown in Fig. 3, and include the modulus of elasticity, thermal expansion, thermal conductivity and heat capacity.

During the machining process, the chip was formed under conditions of elevated temperature, high strains and high strain rates, which significantly influenced the material properties. To model the thermal elastic-plastic behaviour of the medium carbon steel AISI1045, the Johnson-Cook constitutive equation [19-21] was employed.

The tool, made of tungsten carbide, was considered to be a perfectly rigid body and only a heat-transfer analysis was conducted on it. The density was taken as 12700 kg/m^3 , the thermal conductivity, 59 W/mK , and the heat capacity, 15 J/K .

2.3 Chip Fracture criterion

Normalized Cockcroft & Latham's fracture criterion was employed to predict the effect of tensile stress on the chip fracture. This can be expressed as [22]:

$$\int^{\bar{\epsilon}_f} \frac{\sigma^*}{\bar{\sigma}} d\bar{\epsilon} = D \quad (1)$$

Where $\bar{\epsilon}_f$ is the critical damage effective strain, σ^* the maximum tensile stress, $\bar{\sigma}$ the effective stress, $\bar{\epsilon}$ the effective strain and D the material constant. The value of D , usually called damage value, was taken to be 0.3 in this work.

When the integral of the largest tensile principal stress component over the plastic strain path in equation (1) reaches the value of D , fracture occurs or chip fracture starts. During the numerical computation, the critical damage value of each element is calculated at each time-step.

The damage was evaluated for each element of the workpiece. The element deletion occurs when the damage values are satisfied. With the continuous deletion of element, the crack initiation and propagation are obtained. The theoretical assumption was that the critical damage value is a constant for a particular workpiece material and does not depend on the working operation or on the tool material [23]. The critical value was evaluated by a tensile test. During the simulative runs, to obtain results that agreed with the experimental observations, different critical values were used.

2.4 Friction modelling and heat transfer

During experiments, two distinct regions, viz. sticking and sliding region, were observed on the tool/chip interface. Based on the experimental stress distribution on the rake face, an

equivalent shear stress limit was proposed in the sticking region and a constant coefficient of friction in the sliding region. The main heat sources responsible for the high temperature rise during machining processes include: (1) heat generation due to plastic deformation of the workpiece in the primary and secondary deformation zones; (2) heat generated at the tool-chip and tool-workpiece interface due to friction.

As shown in Fig.1 (b), the edges AB, BC of the workpiece and HG, GF of the tool were away from the cutting zone and therefore remained at room temperature. The tool-chip contact (edge KE) was thermally perfect, i.e., a very large value for the tool-chip interface heat transfer coefficient was used. Machining was conducted at ambient temperature while the heat losses from the free edges of the workpiece, chip and tool to the environment, due to convection heat transfer, were considered.

3. RESULTS AND DISCUSSIONS

3.1 Chip breaking process

Modelling of the separation of material ahead of the tool is critical to understand the chip formation process. As the tool advances, all nodes move on the tool surface and the elements may deform strongly. Remeshing procedure was employed to remove materials separated from the workpiece. In this study, the workpiece was remeshed whenever a predefined critical value of tool penetration is reached. A penetration check could be performed at each iteration or at the end of increments. A new boundary of the tool-chip and tool-workpiece interface was deformed after remeshing.

Fig. 3 shows the simulated chip breaking process under the cutting conditions of cutting speed at 60 m/min and feed f at 0.3 mm. Time t indicates the time after the tool contacted the workpiece. The cutting tool initially indented the workpiece ($t = 0$ ms), materials separated from the workpiece formed the chip and then moved up the rake face of the tool. When the chip reached the chip breaker edge ($t = 1$ ms), the force generated by the chip breaker edge was applied to the chip and the curling of the chip resulted ($t = 2\sim 3$ ms). The cutting and feed force during the process of chip flowing and curling can be seen in Fig. 4. It can be observed that a steady state was reached very quickly after the initiation of the cutting process. After the steady state, the cutting force reached a value of 475 N and the feed force was 50 N. The experimental cutting force at steady state under the same cutting conditions is also shown in Fig. 4 and had a value of 536 N. Comparison between the predicted and the experimental cutting force shows an acceptable level of agreement.

During the chip crack initiation and propagation, an appropriate crack criterion is very important for prediction. In this simulation, Normalized Cockcroft & Latham's criterion was employed. When the integral of the largest tensile principal stress component over the plastic strain path in equation (2) reaches the critical value, the chip is weakened locally. The resulting local loss in strength becomes the dominant defect where the chip eventually breaks.

After the chip collision to the workpiece surface ($t = 4$ ms), contact force developed due to the free end of the chip touching the workpiece was applied to the chip, resulting in bending moment acting on the chip. Cutting force increased sharply and then remained stable ($t = 4\sim 5$ ms), with the cutting force at 575 N and the feed force 140 N. When the crack causing chip breaking occurred ($t = 5$ ms) on the inside surface of the chip, cutting force decreased in a short time to the initial value of chip flowing and curling. The crack propagated transversely through the chip. Finally the chip broke when the crack reached the other surface ($t = 6$ ms).

Another two chip breaking processes were predicted by this finite element model. Similar processes of the chip behaviour and cutting force can be observed in Figs. 3 and 4. The

predicted results show that the cutting force varies within a chip breaking cycle and this will help identify the chip breaking event. The cutting force increased ($t = 7$ ms and $t = 11$ ms) sharply with the chip collision to the workpiece surface, followed by a stable state. After the crack initiation ($t = 9$ ms and $t = 12$ ms), the cutting force decreased gradually and finally reached a constant value.

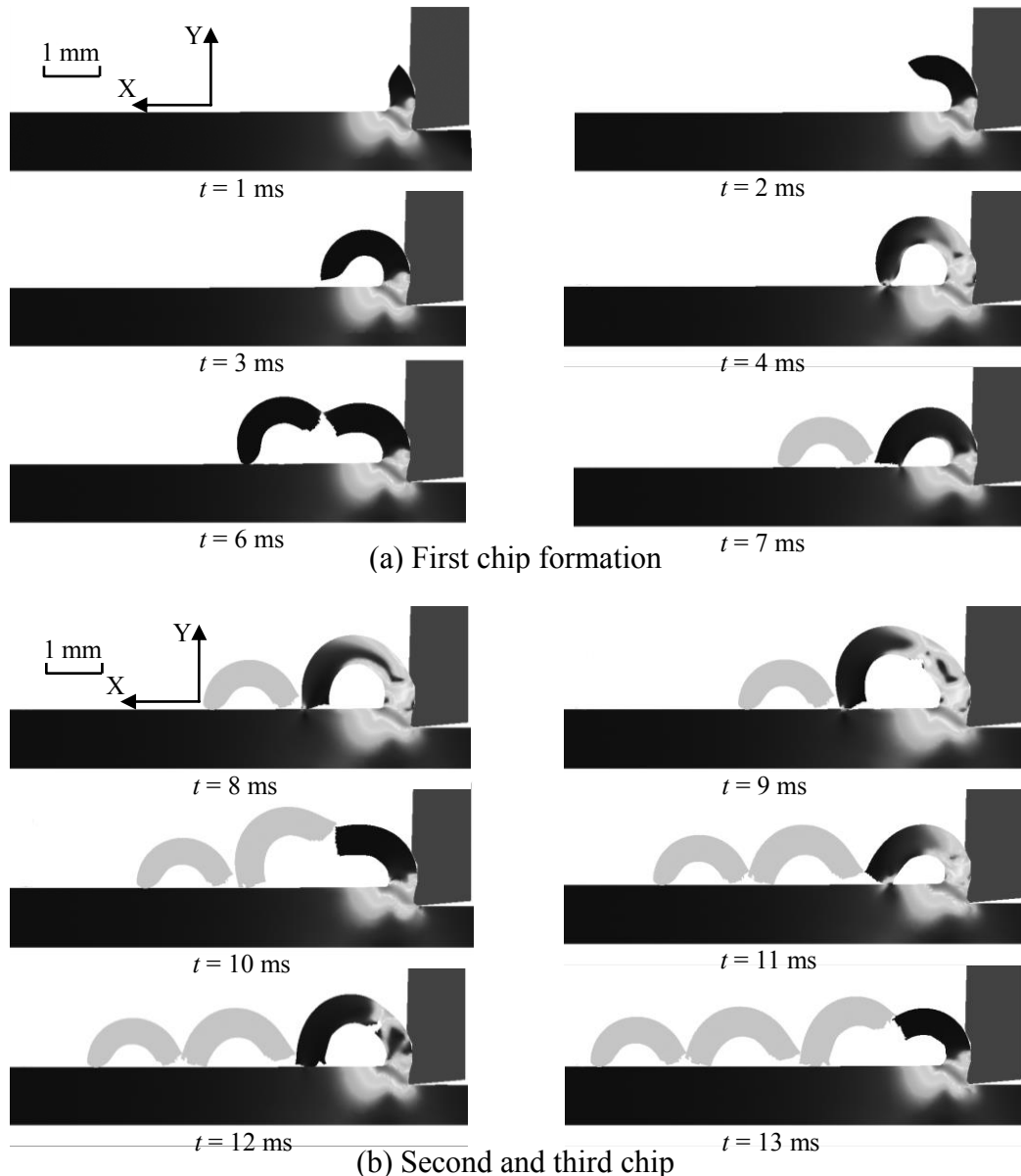


Figure 3: Chip breaking process.

As evidence of the ability of the simulation procedure to model chip breaking, the finite element simulation predictions were compared to the experimental results. The experiment was performed using a lathe. A cutting tool, made of high speed steel, was designed with a chip breaker. The workpiece material was AISI 1045. The cutting tool geometry and cutting parameters were the same as those used for the FEM. As shown in Fig. 5, the characteristics of the chips produced experimentally, with size about $3.6 \times 2.5 \times 0.35$ mm, were in good agreement with those of the FEM. It can be seen that the established chip breaking simulated model is accurate.

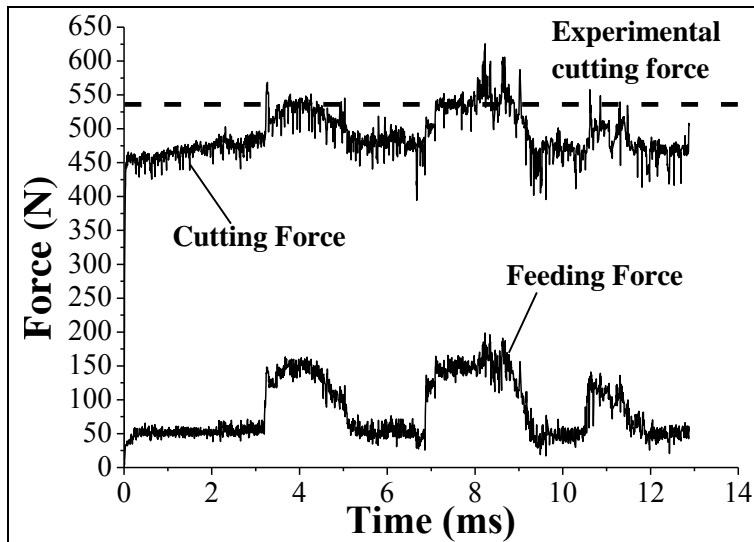


Figure 4: Cutting force and feed force.

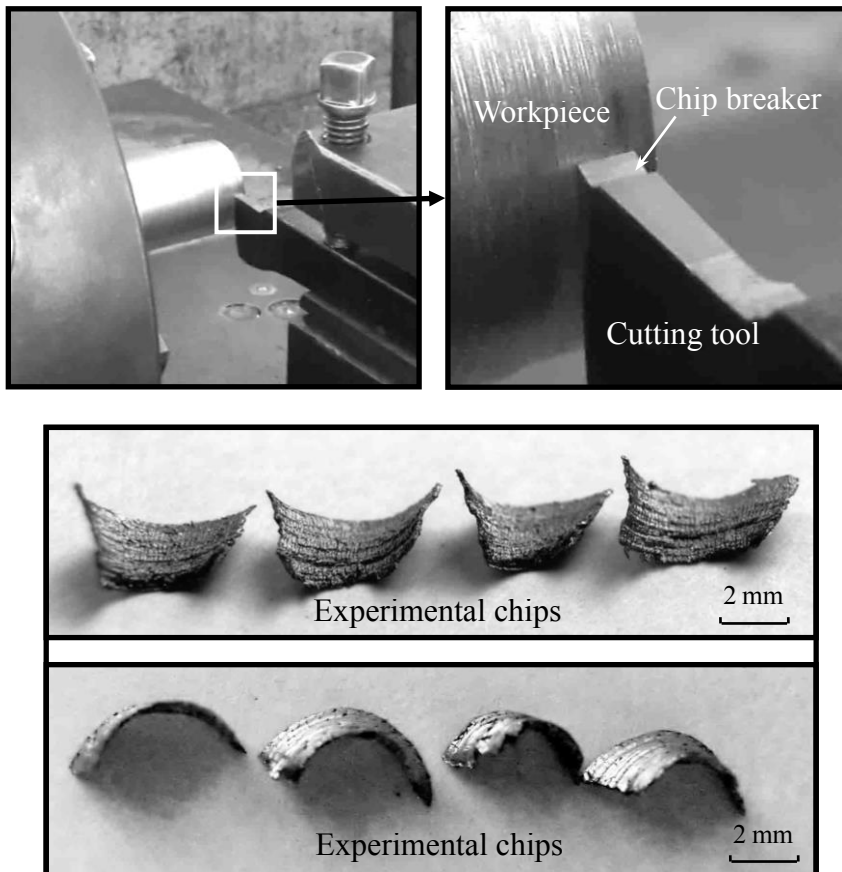


Figure 5: Experimental setup and chips.

3.2 Effective stress

Bending moment on the chip develops after the chip touches the workpiece surface. It increases with chip flow. The chip deforms plastically under the stress on the inside chip surface, which increases with increase in bending moment. Chip deformation is localized around the inside chip surface, resulting in the development of crack on the inner surface of

the chip. The crack grows gradually by the bending moment due to the chip flow. From the above consideration, whether chip is separated or not is strongly dependent on the bending moment acting on the chip.

Fig. 6 shows the effective stress distributions of the chip with time of 4 ms, 5 ms, 9 ms and 12 ms, corresponding to the time when the free end of the chip contacted the workpiece surface and when the crack occurred during the first, second and third broken chip processes. The tensile stress (about 900 MPa) occurs on the inside chip surface where crack occurred and propagated. Stress location can be found around the cutting tool rake face, especially the chip breaker edge. This leads to large strain on the outside chip surface. The maximum effective stress was located at the first deformation zone, with the value of 1190 MPa, 1210 MPa and 1230 MPa for the first, second and third broken chips respectively.

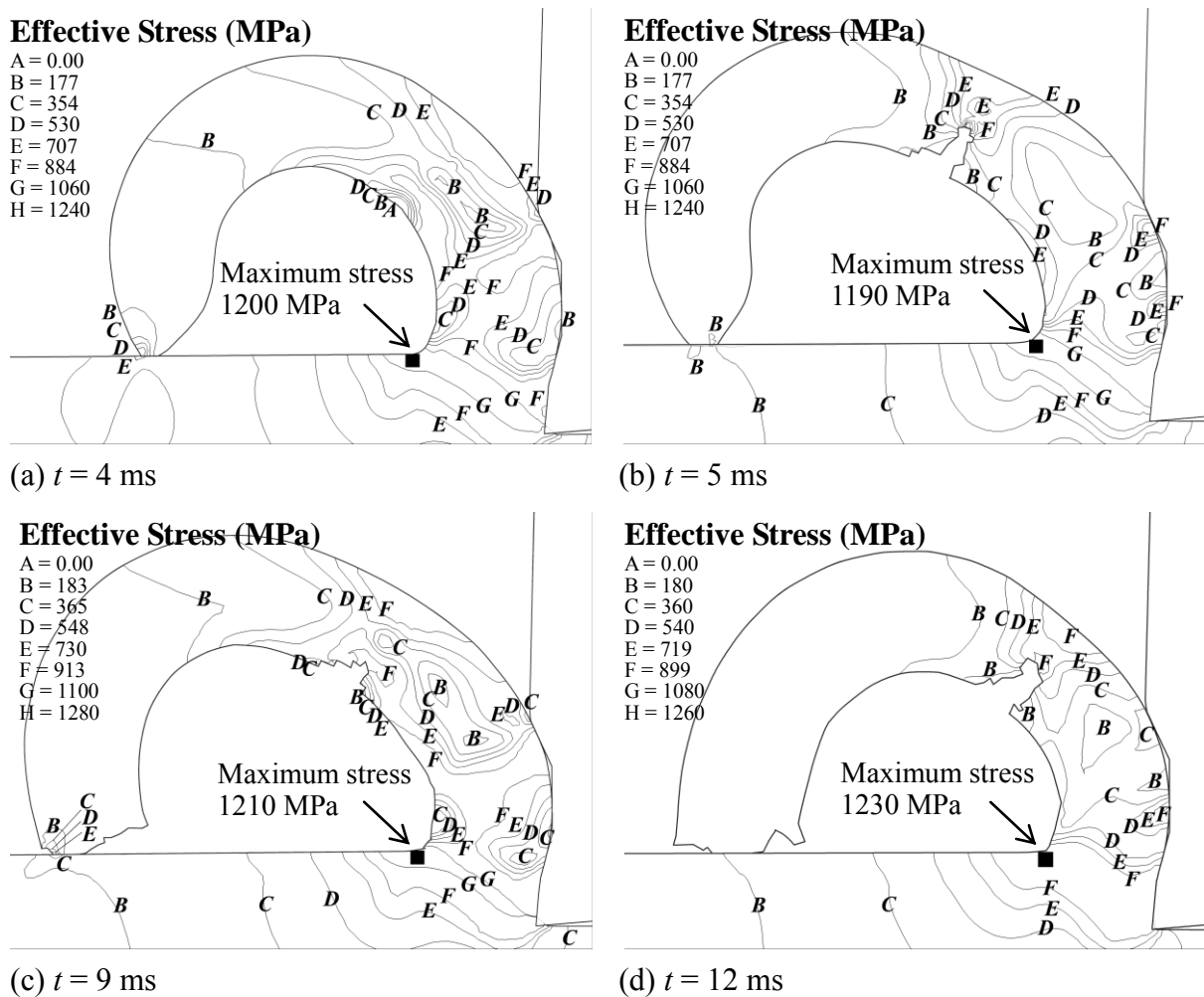


Figure 6: Effective stress distributions of the chip with time of 4 ms, 5 ms, 9 ms and 12 ms.

3.3 Effective strain

The established finite element model also provides an effective method to numerically predict the effective strain in the deformation area. Fig. 7 shows the contours of effective strain distributions of the chip with time of 4 ms, 5 ms, 9 ms and 12 ms.

Plastic strain concentrated around the cutting edge and chip breaker edge in the chip, resulting in high strain on the outer surface of the chip. The maximum effective strain occurred on the outer surface while crack occurred from the inner surface of the chip. The value of the maximum effective strains were 2.67, 2.52 and 2.67 respectively for the first,

second and third chip. The high strain induced material instability in the chip. However, the strain near the inside chip surface was quite small compared to that of the outer chip surface. This also shows the catastrophic plastic deformation that occurred on the outer chip surface.

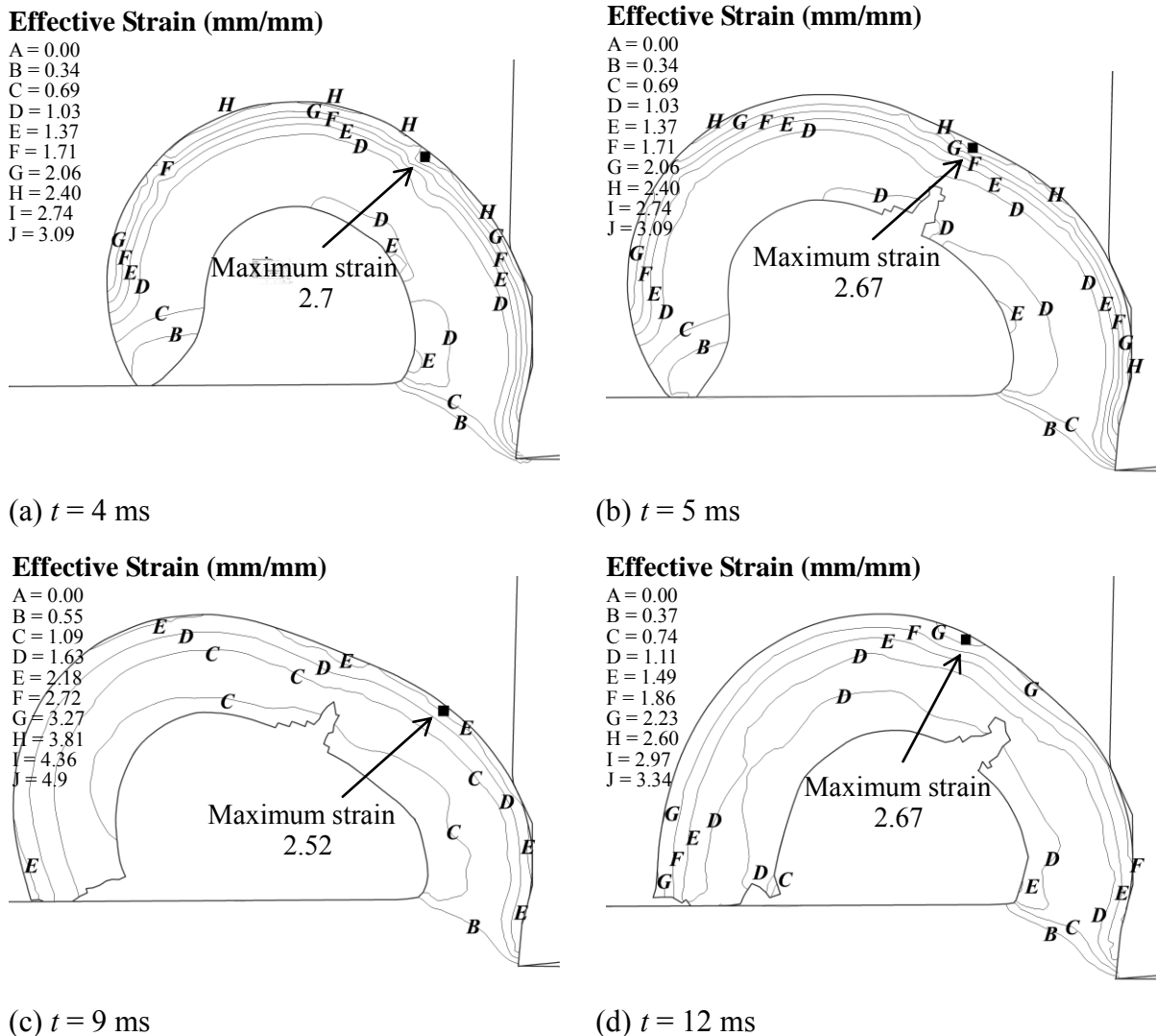


Figure 7: Effective strain distributions of the chip with time of 4 ms, 5 ms, 9 ms and 12 ms.

3.4 Temperature distribution

Heat is generated by friction in the tool-chip interface, resulting in temperature increase. The intense temperature rise induces a secondary deformation zone and creates a metallographic structure unfavourable for chip breaking. This is especially true when the high temperature in the secondary deformation zone reaches or is beyond the crystallization temperature, leading to annealing of the chip in the secondary deformation zone. Furthermore, because the chip flow carries a large portion of the heat generated, the chip bulk temperature tends to rise far beyond the normal working temperature of the workpiece, making the whole chip more ductile than the parent workpiece material. This is quite undesirable from the viewpoint of chip breaking.

For different kinds of cutting operation (finish, medium and rough), there exists a favourable range of contact temperature in the tool-chip interface for acceptable chip breaking.

The value of contact temperature for machining AISI1045 carbon steel in finish cutting operation is 510-650 °C [4].

It is difficult to measure the temperature in the tool-chip interface. Therefore, numerical simulation is an efficient method in the study of the temperature distribution in the tool-chip interface. Fig. 8 shows the temperature distributions in the cutting zone at times 4 ms, 5 ms, 9 ms, and 12 ms. The maximum temperature in the cutting zone occurred at the tool-chip interface, at a distance from the cutting edge of about 0.2 mm. The value of maximum contact temperature was 503 °C for first broken chip, and 509 °C and 480 °C for the second and third broken chips respectively. The temperature in the tool-chip interface is acceptable for the viewpoint of W. Grzesik and E. Kwiatkowska [4]. The location of the maximum temperatures in the chip and tool agreed qualitatively with reported experimental observations [24].

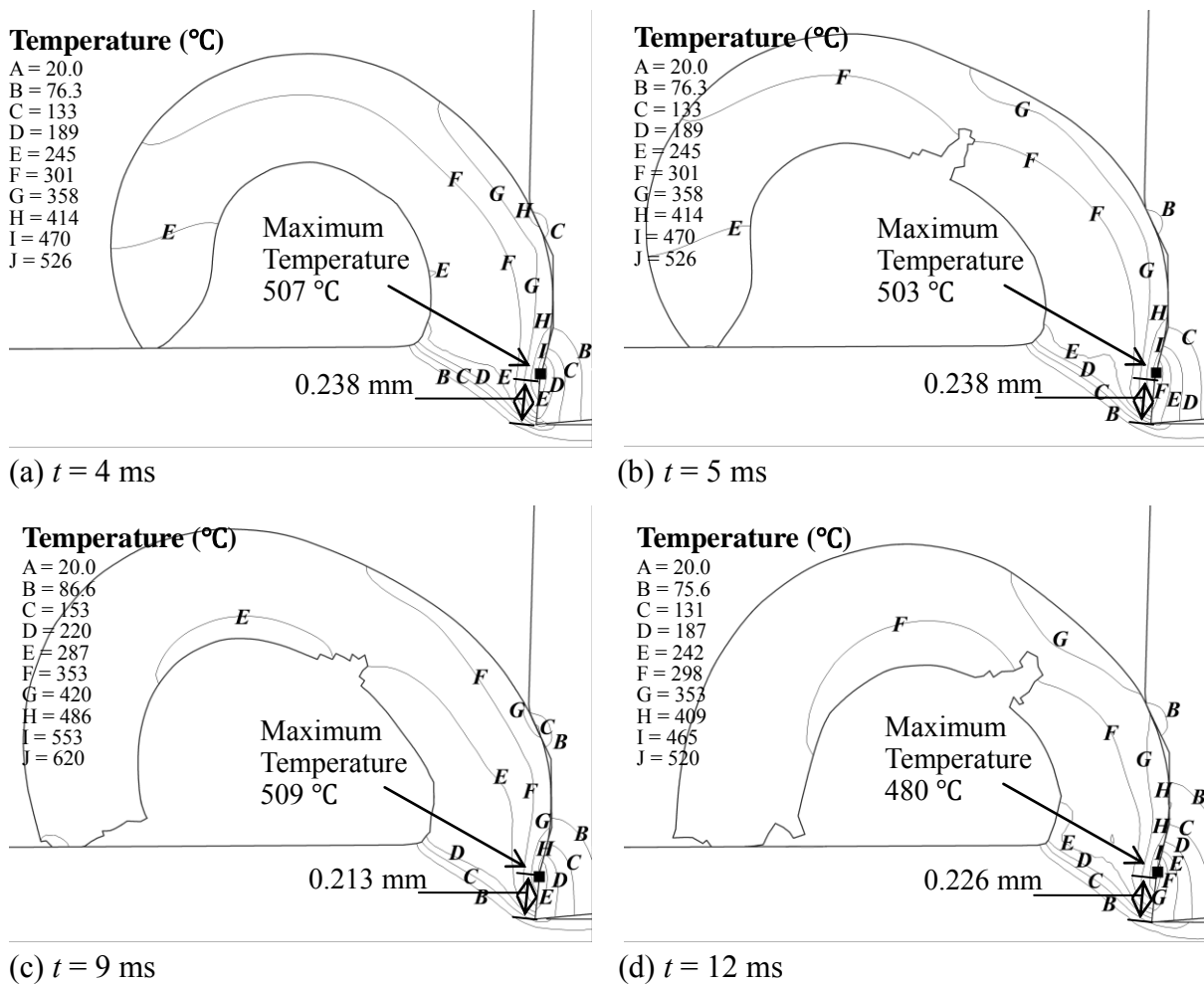


Figure 8: Temperature distribution in the cutting zone with the time of 4 ms, 5 ms, 9 ms, and 12 ms.

4. CONCLUSIONS

The chip breaking process, cutting force and distribution of stress, strain and temperature were investigated by thermo-elastic plastic finite element modelling and simulation. Medium carbon steel AISI1045 was used as workpiece material and high speed steel tool which was considered as perfectly rigid body was employed. Normalized Cockcroft & Latham's criterion

was employed to predict the effect of tensile stress on the chip fracture. The study led to the following conclusions:

(1) The chip breaking process was simulated and broken chip profile was obtained. Cutting force varied within a chip breaking cycle and was useful for identifying the chip breaking event. The simulated broken chip profile and cutting force compared favourably with experimental observations, thus proving that the established FE model can capture the overall trend of the experimental results.

(2) The effective stress was strongly dependent on the bending moment acting on the chip. Large tensile stress occurs (about 900 MPa) on the inside chip surface induced the crack initiation and propagation. The maximum effective stress (about 1200 MPa) was located at the first deformation zone. Compressive stresses around the chip breaker edge developed high strain on the outer chip surface.

(3) Plastic strain concentrated around the cutting edge and chip breaker edge in the chip, resulting in high strain on the outer surface of the chip. The maximum effective strain occurred at the outer surface while crack occurred from the inner surface of the chip, with values of 2.67, 2.52 and 2.67 respectively for the first, second and third chips.

(4) The maximum temperature in the cutting zone occurred at the tool-chip interface, at a distance from the cutting edge of about 0.2 mm. The location of the maximum temperatures in the tool agreed qualitatively with reported experimental observations.

5. ACKNOWLEDGEMENTS

This research was conducted under the support of the National Natural Science Foundation of China (50605022, 51075154), Fundamental Research Funds for the Central Universities (2012ZZ0057), Natural Science Foundation of Guangdong Province (06300160), Zhujiang Science Technology New Stars Foundation (2011J2200066), and Educational Commission of Hubei Province (Q20112602).

REFERENCES

- [1] Jawahir, I. S. (1988). A survey and future predictions for the use of chip breaking in unmanned systems, *International Journal of Advanced Manufacturing Technology*, Vol. 3, No. 4, 87-104, doi:10.1007/BF02601836
- [2] Balaji, A. K.; Ghosh, R.; Fang, X. D.; Stevenson, R.; Jawahir, I. S. (2006). Performance-based predictive models and optimization methods for turning operations and applications: Part 2 – Assessment of chip forms/chip breakability, *Journal of Manufacturing Processes*, Vol. 8, No. 2, 144-158, doi:10.1016/S1526-6125(06)80009-5
- [3] Lee, Y.-M.; Yang, S.-H.; Chang, S.-I. (2006). Assessment of chip-breaking characteristics using new chip-breaking index, *Journal of Materials Processing Technology*, Vol. 173, No. 2, 166-171, doi:10.1016/j.jmatprotec.2005.05.057
- [4] Grzesik, W.; Kwiatkowska, E. (1997). An energy approach to chip-breaking when machining with grooved tool inserts, *International Journal of Machine Tools & Manufacture*, Vol. 37, No. 5, 569-577, doi:10.1016/S0890-6955(96)00076-4
- [5] Kim, J.-D.; Kweun, O.-B. (1997). A chip-breaking system for mild steel in turning, *International Journal of Machine Tools & Manufacture*, Vol. 37, No. 5, 607-617, doi:10.1016/S0890-6955(96)00056-9
- [6] Alvarez, R.; Domingo, R.; Sebastian, M. A. (2011). The formation of saw toothed chip in a titanium alloy: Influence of constitutive models, *Strojniski vestnik – Journal of Mechanical Engineering*, Vol. 57, No. 10, 739-749, doi:10.5545/sv-jme.2011.106

- [7] Fang, N. (1998). Influence of the geometrical parameters of the chip groove on chip breaking performance using new-style chip formers, *Journal of Materials Processing Technology*, Vol. 74, No. 1-3, 268-275, [doi:10.1016/S0924-0136\(97\)00282-3](https://doi.org/10.1016/S0924-0136(97)00282-3)
- [8] Zhou, L.; Rong, Y. M.; Li, Z. J.; Yang, J. A. (2003). Development of web-based machining chip breaking prediction systems, *International Journal of Advanced Manufacturing Technology*, Vol. 22, No. 5-6, 336-343, [doi:10.1007/s00170-002-1496-7](https://doi.org/10.1007/s00170-002-1496-7)
- [9] Puh, F.; Segota, T.; Jurkovic, Z. (2012). Optimization of hard turning process parameters with PCBN tool based on the Taguchi method, *Technical Gazette*, Vol. 19, No. 2, 415 -419
- [10] Athavale, S. M.; Strenkowski, J. S. (1997). Material damage-based model for predicting chip-breakability, *Journal of Manufacturing Science and Engineering*, Vol. 119, No. 4B, 675-680, [doi:10.1115/1.2836808](https://doi.org/10.1115/1.2836808)
- [11] Kamiya, M.; Yakou, T. (2008). Role of second-phase particles in chip breakability in aluminum alloys, *International Journal of Machine Tools & Manufacture*, Vol. 48, No. 6, 688-697, [doi:10.1016/j.ijmachtools.2007.10.018](https://doi.org/10.1016/j.ijmachtools.2007.10.018)
- [12] Joshi, S. S.; Ramakrishnan, N.; Ramakrishnan, P. (1999). Analysis of chip breaking during orthogonal machining of Al/SiCp composites, *Journal of Materials Processing Technology*, Vol. 88, No. 1-3, 90-96, [doi:10.1016/S0924-0136\(98\)00379-3](https://doi.org/10.1016/S0924-0136(98)00379-3)
- [13] Gyliene, V.; Ostasevicius, V. (2012). Modeling and simulation of a chip load acting on a single milling tool insert, *Strojniski vestnik – Journal of Mechanical Engineering*, Vol. 58, No. 12, 716-723, [doi:10.5545/sv-jme.2011.356](https://doi.org/10.5545/sv-jme.2011.356)
- [14] Tamizharasan, T.; Senthil Kumar, N. (2012). Optimization of cutting insert geometry using DEFORM-3D: numerical simulation and experimental validation, *International Journal of Simulation Modelling*, Vol. 11, No. 2, 65-76, [doi:10.2507/IJSIMM11\(2\)1.200](https://doi.org/10.2507/IJSIMM11(2)1.200)
- [15] Chaari, R.; Abdennadher, M.; Louati, J.; Haddar, M. (2011). Modelling of the 3D machining geometric defects accounting for workpiece vibratory behaviour, *International Journal of Simulation Modelling*, Vol. 10, No. 2, 66-77, [doi:10.2507/IJSIMM10\(2\)2.173](https://doi.org/10.2507/IJSIMM10(2)2.173)
- [16] Ganapathy, B. K.; Jawahir, I. S. (1998). Modeling the chip-work contact force for chip breaking in orthogonal machining with a flat-faced tool, *Journal of Manufacturing Science and Engineering*, Vol. 120, No. 1, 49-56, [doi:10.1115/1.2830110](https://doi.org/10.1115/1.2830110)
- [17] Fang, X. D.; Jawahir, I. S. (1996). An analytical model for cyclic chip formation in 2-D machining with chip breaking, *CIRP Annals – Manufacturing Technology*, Vol. 45, No. 1, 53-58, [doi:10.1016/S0007-8506\(07\)63016-9](https://doi.org/10.1016/S0007-8506(07)63016-9)
- [18] Shinozuka, J.; Obikawa, T.; Shirakashi, T. (1996). Chip breaking analysis from the viewpoint of the optimum cutting tool geometry design, *Journal of Materials Processing Technology*, Vol. 62, No. 4, 345-351, [doi:10.1016/S0924-0136\(96\)02433-8](https://doi.org/10.1016/S0924-0136(96)02433-8)
- [19] Sima, M.; Ozel, T. (2010). Modified material constitutive models for serrated chip formation simulations and experimental validation in machining of titanium alloy Ti-6Al-4V, *International Journal of Machine Tools & Manufacture*, Vol. 50, No. 11, 943-960, [doi:10.1016/j.ijmachtools.2010.08.004](https://doi.org/10.1016/j.ijmachtools.2010.08.004)
- [20] Calamaz, M.; Coupard, D.; Girod, F. (2008). A new material model for 2D numerical simulation of serrated chip formation when machining titanium alloy Ti-6Al-4V, *International Journal of Machine Tools & Manufacture*, Vol. 48, No. 3-4, 275-288, [doi:10.1016/j.ijmachtools.2007.10.014](https://doi.org/10.1016/j.ijmachtools.2007.10.014)
- [21] Rhim, S.-H.; Oh, S.-I. (2006). Prediction of serrated chip formation in metal cutting process with new flow stress model for AISI 1045 steel, *Journal of Materials Processing Technology*, Vol. 171, No. 3, 417-422, [doi:10.1016/j.jmatprotec.2005.08.002](https://doi.org/10.1016/j.jmatprotec.2005.08.002)
- [22] Cockroft, M. G.; Latham, D. J. (1968). Ductility and the workability of metals, *Journal of Institute of Metals*, Vol. 96, 33 -39
- [23] Oh, S. I.; Chen, C. C.; Kobayashi, S. (1979). Ductile fracture in axisymmetric extrusion and drawing – Part 2: Workability in extrusion and drawing, *Journal of Engineering for Industry*, Vol. 101, No. 1, 36-44, [doi:10.1115/1.3439471](https://doi.org/10.1115/1.3439471)
- [24] Lin, Z.-C.; Lo, S.-P. (1997). Ultra-precision orthogonal cutting simulation for oxygen-free high-conductivity copper, *Journal of Materials Processing Technology*, Vol. 65, No. 1-3, 281-291, [doi:10.1016/S0924-0136\(96\)02416-8](https://doi.org/10.1016/S0924-0136(96)02416-8)